

Can Channels be Fully Inferred Between Two Antenna Panels?

Yuelong Qiu, Di Wu, and Yong Zeng, *Senior Member, IEEE*

Abstract—This letter considers a two-panel massive multiple-input multiple-output (MIMO) communication system, where the base station (BS) is equipped with two antenna panels that may use different frequency bands for communication. By exploiting the geometric relationships between antenna panels, efficient channel inference methods across antenna panels are proposed to reduce the overhead of real-time channel estimation. Four scenarios are considered, namely far-field free-space, near-field free-space, multi-path sharing far-field scatterers, and multi-path sharing near-field scatterers. For both far-field and near-field free-space scenarios, we show that the channel of one panel can be fully inferred from that of the other panel, as long as the multi-path components (MPCs) composing the channel can be resolved. On the other hand, for the multi-path scenarios sharing far-field or near-field scatterers, only the angles or range of angles of the MPCs can be inferred, respectively. Simulation results based on commercial 3D ray-tracing software are presented to validate our developed channel inference techniques.

Index Terms—channel inference, two-panel massive MIMO, CSI acquisition.

I. INTRODUCTION

Massive multiple-input multiple-output (MIMO) is one of the key technologies for enabling millimeter wave (mmWave) communications [1]. To reduce the hardware cost and power consumption of massive MIMO systems, the 3rd Generation Partnership Project (3GPP) has proposed the use of antenna in package (AIP) technology. Specifically, AIP juxtaposes multiple antenna panels to form multi-panel massive MIMO [2]. As a partially-connected hybrid architecture, each antenna panel in the multi-panel massive MIMO system is linked to a modest number of radio frequency (RF) chains, resulting in significant reductions in hardware costs and energy consumption [3]. This has made the system increasingly popular in the industry, especially in high-frequency bands [4]. However, the large antenna array composed of multiple antenna panels are typically non-uniform in structure, meaning that the distance between adjacent panels is much greater than the distance between adjacent antenna elements [2]. The cost of channel state information (CSI) acquisition is increased in multi-panel massive MIMO systems due to two factors. Firstly, the presence of multiple antenna panels requires the acquisition of more CSI as compared to one single panel. Secondly, due to the large inter-panel separations, different antenna panels may have different channel parameters, such as number

of multi-paths, angles of arrivals/departures (AoAs/AoDs). A potential solution to reduce CSI acquisition overhead is channel extrapolation, which tries to infer the CSI of one antenna panel based on that of another one.

There have been extensive studies on channel extrapolation, which can be classified into time-, frequency-, and spatial-domain extrapolation. For time-domain channel extrapolation, current research mainly focuses on time division duplexing (TDD) systems [5]. For frequency-domain channel extrapolation, some studies tried to achieve extrapolation within Sub-6 GHz or from Sub-6 GHz to mmWave [6], [7]. For spatial-domain channel extrapolation, most research mainly focuses on channel extrapolation between different antennas on the same panel [8], while channel extrapolation between different base stations (BSs) and different panels is rare [9], [10]. Furthermore, artificial intelligence (AI)-based time-, frequency- and spatial-domain channel extrapolation is discussed in [11]. Additionally, a novel concept termed channel knowledge map (CKM) was recently proposed [12], [13], which can enhance environment-awareness and facilitate CSI acquisition by utilizing location and environment information.

In this letter, we consider a two-panel massive MIMO communication system, where the BS is equipped with two antenna panels for communication. The main objective is to infer the channel of one panel using that of the other panel. Unlike the multi-panel scenario considered by 3GPP, where the antenna panels mainly operate in the same frequency band [2], [4], we consider the more general scenario that the panels may use different frequency bands. Moreover, since the separation between panels is larger than that between antenna elements within a panel, channel inference across antenna panels is more challenging than channel extrapolation between antenna elements on the same panel. Fortunately, by exploiting the geometric structure between antenna panels at the BS, we show that the channel of one panel can be in principle fully inferred from that of the other panel for both far-field and near-field free-space scenarios, as long as the multi-path components (MPCs) composing the channel can be resolved. On the other hand, for the multi-path scenarios sharing far-field or near-field scatterers, only the angles or range of angles of the MPCs can be inferred, respectively. Numerical results based on commercial ray tracing software are provided to validate our analysis.

II. SYSTEM MODEL

As shown in Fig. 1, we consider a downlink wireless communication system where the BS is equipped with two antenna panels, denoted as Panel₁ and Panel₂, and their

This work was supported by the National Key R&D Program of China with grant number 2019YFB1803400, in part by the National Natural Science Foundation of China with grant number 62071114.

The authors are with the National Mobile Communications Research Laboratory, Southeast University, Nanjing 210096, China.

Yong Zeng is also with the Purple Mountain Laboratories, Nanjing 211111, China (e-mail: yl_qiu, studywudi, yong_zeng@seu.edu.cn).

operating frequencies are denoted as f_1 and f_2 , respectively. Panel₁ and Panel₂ are placed in the same vertical plane, with their bottom edges having heights d_1 and d_2 , respectively. Both Panel₁ and Panel₂ are uniform planar arrays (UPAs) with adjacent antenna elements separated by half wavelength. The bottom-left antenna elements of Panel₁ and Panel₂ are chosen as their reference elements, respectively. The total number of antenna elements in Panel₁ is $N_1 = N_{z_1}N_{y_1}$, where N_{z_1} and N_{y_1} are the number of elements in the z-axis and y-axis, respectively. Similarly, the number of antenna elements in Panel₂ is $N_2 = N_{z_2}N_{y_2}$. Furthermore, the distance between the reference antenna elements of Panel₁ and Panel₂ is denoted as Δd , and the overall maximum dimension formed by Panel₁ and Panel₂ is denoted by D , as illustrated in Fig. 1.

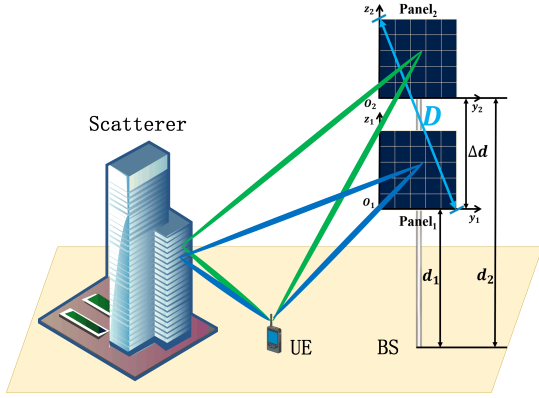


Fig. 1. Wireless communication where the BS is equipped with two antenna panels.

We assume that the user equipment (UE) and scatterers are at the far-field of each panel, but may be located in the near-field of the overall aperture D formed by the two panels. Therefore, the channel vectors between Panel_k and a single-antenna UE can be expressed as

$$\mathbf{h}_k = \sqrt{N_k} \sum_{l=1}^{L_k} \alpha_l(\lambda_k) \mathbf{a}_k(\theta_{l,k}, \phi_{l,k}), k = 1, 2, \quad (1)$$

where L_k is the total number of paths, $\alpha_l(\lambda_k)$ is the complex gain of path l whose value depends on the carrier wavelength $\lambda_k = c/f_k$, with c being the speed of light and f_k being the frequency, $\mathbf{a}_k(\cdot)$ is the steering vector of the antenna array at Panel_k, and $\theta_{l,k} \in [-\frac{\pi}{2}, \frac{\pi}{2}]$ and $\phi_{l,k} \in [0, 2\pi)$ are the elevation and azimuth angles of path l of Panel_k, respectively.

With adjacent elements separated by half-wavelength for both antenna panels, the array steering vector for angle (θ, ϕ) can be expressed as

$$\mathbf{a}_k(\theta, \phi) = \mathbf{a}_{y_k}(\theta, \phi) \otimes \mathbf{a}_{z_k}(\theta), \quad (2)$$

where

$$\mathbf{a}_{y_k}(\theta, \phi) = \frac{1}{\sqrt{N_{y_k}}} [1, e^{j\pi \cos(\theta) \sin(\phi)}, \dots, e^{j\pi(N_{y_k}-1) \cos(\theta) \sin(\phi)}]^T, \quad (3)$$

$$\mathbf{a}_{z_k}(\theta) = \frac{1}{\sqrt{N_{z_k}}} [1, e^{j\pi \sin(\theta)}, \dots, e^{j\pi(N_{z_k}-1) \sin(\theta)}]^T. \quad (4)$$

For the same UE, each antenna panel needs to obtain its own CSI. To reduce the CSI acquisition overhead for two-panel systems, we exploit the geometric relationship between panels

to achieve channel inference from \mathbf{h}_1 to \mathbf{h}_2 . As such, only CSI of \mathbf{h}_1 needs to be estimated in real-time. To that end, we make the following assumption:

Assumption 1: The multi-path parameters $\alpha_l(\lambda_1)$, $\theta_{l,1}$, and $\phi_{l,1}$, $l = 1, \dots, L_1$, can be obtained based on the channel vector \mathbf{h}_1 .

Assumption 1 is valid if Panel₁ has a sufficiently large antenna number N_1 and/or the channel is sparse, so that $L_1 \ll N_1$. In this case, one may use algorithms like multiple signal classification (MUSIC) [14], space-alternating generalized expectation-maximization (SAGE) [15], or compressive sensing to extract the multi-path parameters based on the channel. As such, the process of inferring \mathbf{h}_2 from \mathbf{h}_1 can be divided into three phases. Firstly, according to Assumption 1, obtain the multi-path parameters $\alpha_l(\lambda_1)$, $\theta_{l,1}$, and $\phi_{l,1}$ of the known channel vector \mathbf{h}_1 . Secondly, infer the multi-path channel parameters $\alpha_l(\lambda_2)$, $\theta_{l,2}$, and $\phi_{l,2}$ of \mathbf{h}_2 according to the geometric relationship between Panel₁ and Panel₂. Finally, reconstruct the channel vector \mathbf{h}_2 based on the inferred multi-path parameters. In fact, Assumption 1 is not a must if instead of estimating the composite channel \mathbf{h}_1 , the aforementioned multi-path parameters are directly estimated at the first place for Panel₁. This is usually the case for integrated sensing and communication (ISAC) systems [16]. Since the other two steps are either well studied or straightforward, this letter mainly focuses on the second step, i.e., inferring $\alpha_l(\lambda_2)$, $\theta_{l,2}$, and $\phi_{l,2}$ from $\alpha_l(\lambda_1)$, $\theta_{l,1}$, and $\phi_{l,1}$.

III. CHANNEL INFERENCE ACROSS PANELS

To distinguish between far-field from near-field scenarios, the classical Rayleigh distance is defined as $r_{Rayl} = \frac{2D^2}{\lambda}$ [17], where D is the overall aperture of Panel₁ and Panel₂, and $\lambda = \min\{\lambda_1, \lambda_2\}$. Denote the distance between the UE and the reference antenna elements of Panel₁ and Panel₂ as R_1 and R_2 , respectively, and let $r = \min\{R_1, R_2\}$. When $r \geq r_{Rayl}$, UE is in the far-field of the antenna panels, and Panel₁ and Panel₂ would share the same multi-path parameters, such as number of multi-paths and their AoDs [18]; otherwise, UE is in the near-field and Panel₁ and Panel₂ would have different multi-path parameters [17].

A. Far-field Free-Space

In far-field free-space scenarios, there is only one line of sight (LoS) path, i.e., $L_k = 1$, so that the channel vectors in (1) are simplified to

$$\mathbf{h}_k = \sqrt{N_k} \alpha(\lambda_k) \mathbf{a}_k(\theta_k, \phi_k), k = 1, 2. \quad (5)$$

Therefore, the channel vector \mathbf{h}_2 can be inferred from \mathbf{h}_1 if the parameters $\alpha(\lambda_2)$, θ_2 and ϕ_2 of Panel₂ can be inferred from $\alpha(\lambda_1)$, θ_1 and ϕ_1 .

As UE is in the far-field of the overall aperture D formed by both panels, the AoDs for Panel₁ and Panel₂ are equal, so that $\theta_2 = \theta_1$ and $\phi_2 = \phi_1$. Furthermore, based on Friis transmission equation, the complex-valued channel gain $\alpha(\lambda_k)$ can be written as

$$\alpha(\lambda_k) = \frac{\lambda_k}{4\pi R_k} e^{-\frac{j2\pi R_k}{\lambda_k}}, k = 1, 2, \quad (6)$$

where R_k is the distance from the UE to the reference antenna element of Panel_k.

Since R_1 and R_2 are larger than the classical Rayleigh distance, the approximation $R_1 \approx R_2$ can be used when evaluating the amplitude of $\alpha(\lambda_2)$. However, the phase calculation needs to consider the wavelength and the distance of the signal to Panel₂. It can be shown that $\alpha(\lambda_2)$ can be inferred from $\alpha(\lambda_1)$ as

$$\alpha(\lambda_2) = |\alpha(\lambda_1)| \frac{\lambda_2}{\lambda_1} \left(\frac{\alpha(\lambda_1)}{|\alpha(\lambda_1)|} \right)^{\frac{\lambda_1}{\lambda_2}} e^{\frac{j2\pi\Delta d \sin(\theta_2)}{\lambda_2}}, \quad (7)$$

where $|\cdot|$ is the modulus operation for complex numbers, Δd is the distance between the reference antenna elements of Panel₁ and Panel₂ as shown in Fig. 1.

Proof: Please refer to Appendix A. ■

Therefore, from the above analysis, we can obtain the following theorem:

Theorem 1: In the far-field free-space scenario, \mathbf{h}_2 can be fully inferred from \mathbf{h}_1 by using $\theta_2 = \theta_1$, $\phi_2 = \phi_1$, and $\alpha(\lambda_2)$ in (7).

B. Near-field Free-Space

When the UE is in the near-field of the overall aperture D , the AoDs of Panel₁ and Panel₂ are different in general, as illustrated in Fig. 2. By exploiting the geometric relationship between the two panels, it is not difficult to infer the AoD θ_2 based on θ_1 , given by

$$\theta_2 = \tan^{-1} \left(\frac{d_2}{d_1} \tan \theta_1 \right). \quad (8)$$

Besides, since Panel₁ and Panel₂ are in the same vertical plane, the azimuth AoDs of both panels are equal, i.e., $\phi_2 = \phi_1$.

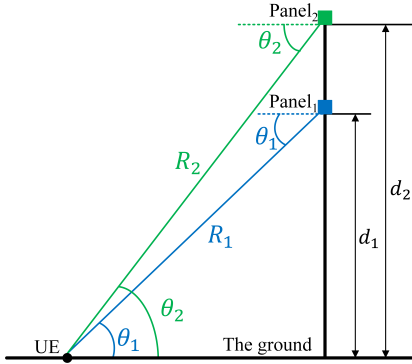


Fig. 2. Geometric relation between two panels in near-field free-space.

Furthermore, with θ_2 obtained in (8), the distance R_2 from UE to reference antenna element of Panel₂ can be obtained as

$$R_2 = \frac{d_2}{|\sin \theta_2|}. \quad (9)$$

Thus, the complex-valued gain $\alpha(\lambda_2)$ can be obtained by substituting R_2 into (6).

Theorem 2: In the near-field free-space scenario, \mathbf{h}_2 can be fully inferred from \mathbf{h}_1 by using $\phi_2 = \phi_1$, θ_2 in (8), and $\alpha(\lambda_2)$ in (6).

C. Multi-path Sharing Far-field Scatterers

For multi-path scenarios, let S_l denote the locations of scatterer l , which are assumed to be shared by both panels. In the far-field scenario, S_l are in the far-field of the overall aperture D , so that the AoDs of Panel₁ and Panel₂ of the

multi-paths are equal, i.e., $L_1 = L_2$, and $\theta_{l,2} = \theta_{l,1}$ and $\phi_{l,2} = \phi_{l,1}, \forall l$.

However, it is difficult to infer the path gain $\alpha_l(\lambda_2)$ from $\alpha_l(\lambda_1)$ since the scattered power loss and phase shift when the signal interacts with the scatterers depend on the scatterer surface material in a sophisticated manner. Nevertheless, the inferred angle information is highly valuable to facilitate the estimation of \mathbf{h}_2 . One possible approach is by combining the inferred angle information with a small amount of real-time training [19].

Theorem 3: In the multi-path sharing far-field scatterers scenario, AoDs of the MPCs of \mathbf{h}_2 can be inferred by using $\theta_{l,2} = \theta_{l,1}$, and $\phi_{l,2} = \phi_{l,1}$.

D. Multi-path Sharing Near-field Scatterers

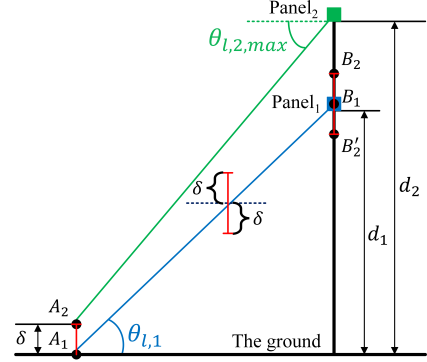


Fig. 3. Geometric relation between two panels in multi-path scenario sharing near-field scatterers.

For multi-path scenarios when the scatterers S_l are in the near-field of the overall aperture D , the elevation AoDs of the MPCs are in general different for the two panels, as illustrated in Fig. 3. Although we cannot determine the exact location of scatterer S_l , based on the AoD $\theta_{l,1}$ of Panel₁, the scattering point of Panel₁ must be located at a point along the line segment A_1B_1 shown in Fig. 3. Furthermore, in practice, there is usually a slight deviation in the exact scattering point of Panel₂. Specifically, the scattering point of Panel₂ may vertically deviate from that of Panel₁ by a maximum value of δ , as illustrated in Fig. 3. Therefore, the range of $\theta_{l,2}$ can be determined by considering two extreme cases. Specifically, if the scattering point of Panel₁ is located at the furthest point along direction $\theta_{l,1}$, i.e., point A_1 , and the scattering point of Panel₂ is located at point A_2 . Then the maximum value of $\theta_{l,2}$ is

$$\theta_{l,2,\max} = \tan^{-1} \left(\frac{d_2 - \delta}{d_1} \tan \theta_{l,1} \right). \quad (10)$$

If the scattering point of Panel₁ is located at point B_1 , it is obvious that $\theta_{l,2,\min} = -\frac{\pi}{2}$, irrespective of the location of the scattering point of Panel₂ along the line segment $B_2B'_2$ shown in Fig. 3. Therefore, the range of $\theta_{l,2}$ is $\left(-\frac{\pi}{2}, \tan^{-1} \left(\frac{d_2 - \delta}{d_1} \tan \theta_{l,1} \right) \right]$. It is obvious that the larger δ is, the wider the range of $\theta_{l,2}$, i.e., less information is inferred for Panel₂. Therefore, in practice, there is a tradeoff for selecting the values of δ .

Theorem 4: In the multi-path sharing near-field scatterers scenario, the azimuth AoDs and the range of elevation AoDs

of MPCs of \mathbf{h}_2 can be inferred by using $\phi_{l,2} = \phi_{l,1}$, and $\theta_{l,2} \in \left(-\frac{\pi}{2}, \tan^{-1}\left(\frac{d_2-\delta}{d_1}\tan\theta_{l,1}\right)\right]$.

Based on the above analysis, the results of channel inference across antenna panels under different scenarios are summarized in Table I. Note that for the most complex scenarios where the multi-path scatterers of different panels are different, it is very challenging to directly infer useful channel knowledge across panels. In this case, the technique of CKM [12], [13] might be useful since it utilizes the location and environment information of the actual propagation environment.

TABLE I

SUMMARY OF INTER-PANEL CHANNEL INFERENCE UNDER DIFFERENT SCENARIOS.

Scenarios	Inference results
Far-field free-space	\mathbf{h}_2 can be completely inferred.
Near-field free-space	
Multi-path sharing far-field scatterers	$\phi_{l,2}$ and $\theta_{l,2}$ can be inferred.
Multi-path sharing near-field scatterers	$\phi_{l,2}$ and the range of $\theta_{l,2}$ can be inferred.
Multi-path with different scatterers	Challenging to directly infer useful channel knowledge across panels. May use CKM.

IV. SIMULATION RESULTS

In this section, the discussed channel inference techniques under different scenarios are verified through ray-tracing simulation. The commercial ray tracing software Remcom Wireless Insite¹ is used to generate the ground-truth channel information. Panel₁ and Panel₂ are 16×16 UPAs, with $f_1 = 28$ GHz and $f_2 = 39$ GHz, respectively. The height of Panel₁ is fixed to $d_1 = 15$ meters, while d_2 varies among 16, 18 and 20 meters.

A. Free-Space scenarios

For both far-field and near-field free-space scenarios, \mathbf{h}_2 can be in principle fully inferred from \mathbf{h}_1 . Let \mathbf{h}_2 and $\hat{\mathbf{h}}_2$ denote the true and inferred channel vectors, respectively. Then we use the following correlation coefficient to evaluate the quality of inference:

$$F = \frac{|\hat{\mathbf{h}}_2^H \mathbf{h}_2|^2}{\|\hat{\mathbf{h}}_2\|^2 \|\mathbf{h}_2\|^2}. \quad (11)$$

Note that F is a highly relevant metric for channel inference if the inferred result is mainly used for multi-antenna beamforming. Specifically, with Cauchy-Swartz inequality, it is not difficult to see that F takes the value between 0 and 1, and the higher its value, the better the channel inference for beamforming gain. Fig. 4 shows the correlation coefficient in far-/near-field free-space scenario with three different panel spacings: 1 m, 3 m, and 5 m. According to $r_{Rayl} = \frac{2D^2}{\lambda}$, the near-field range increases with the panel spacing. Therefore, even with an increase in panel spacing, the inference method in near-field free-space scenario can maintain a good inference quality. However, for the method in far-field free-space scenario, the overall inference quality drops with an increase in panel spacing. Note that the elevation angle θ and azimuth angle ϕ are the main factors that determine F . However, due to the geometric relationship between Panel₁ and Panel₂, only

the value of θ changes significantly. Therefore, the change of F mainly depends on the inference accuracy of θ . According to the inference method in the far-field free-space scenario, we can conclude that the estimated value $\hat{\theta}_2$ of θ_2 satisfies $\hat{\theta}_2 = \theta_1$. If the horizontal distance between UE and BS is d_x , according to the geometric relationship in Fig. 2, the inference error of θ_2 is

$$\begin{aligned} \Delta\theta_2 &= |\theta_2 - \hat{\theta}_2| = |\theta_2 - \theta_1| = \tan^{-1}\left(\frac{d_2}{d_x}\right) - \tan^{-1}\left(\frac{d_1}{d_x}\right) \\ &= \tan^{-1}\left(\frac{d_x(d_2 - d_1)}{d_x^2 + d_1 d_2}\right), \end{aligned} \quad (12)$$

where $\Delta\theta_2$ firstly increases and then decreases as d_x increases. Therefore, for the inference method in the far-field free-space scenario, the F decreases first and then increases.

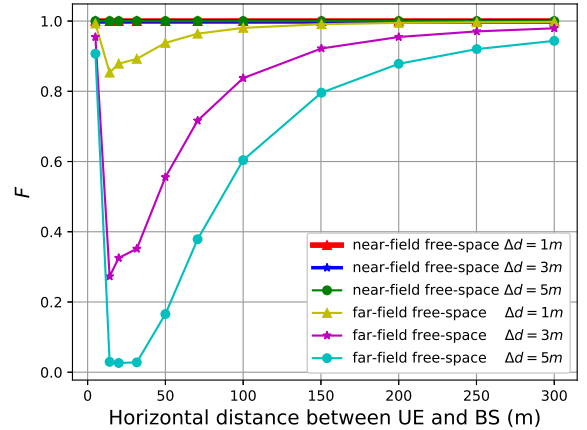


Fig. 4. Comparison of channel correlation coefficient for the inference methods in far-/near-field free-space scenario with three different panel spacings.

B. Multi-path scenarios

Fig. 5 shows the actual diffuse scattering environment of the multi-path scenario, with the diffuse scattering factor set to 0.2. The entire area contains 4848 UE locations, and the maximum number of MPCs is 25 when configuring Wireless Insite of Remcom. These UEs have a total of 95850 and 93591 MPCs between Panel₁ and Panel₂, respectively. Consider the MPCs that have common scatterers between Panel₁ and Panel₂. Then, a total of 85673 MPCs meet this criterion, which account for 89.4% and 91.5% of the total MPCs for Panel₁ and Panel₂, respectively. In the simulation, we set $\delta = 0.15$ meters and only consider the 85673 selected MPCs. In the scene depicted in Fig. 5, utilizing the inference method in multi-path sharing far-field scatterers scenario to infer the value of $\theta_{l,2}$, i.e. $\theta_{l,2} = \theta_{l,1}$, the average inference error for the entire region is 1.52° . For multi-path sharing near-field scatterers scenario, since there is no prior information of the exact location of scatterers S_l , only the range of $\theta_{l,2}$ can be obtained. In Fig. 6, the purple pentagon represents the position of the BS and the dark red areas are the buildings/vegetation/pond. The value at each UE location is the proportion of the number of MPCs with correctly inferred $\theta_{l,2}$ to the total number of MPCs with common scatterers between Panel₁ and Panel₂ at that location. It can be observed that utilizing the inference

¹<https://www.remcom.com/wireless-insite-em-propagation-software>

method in the multi-path sharing near-field scatterers scenario, an accuracy over 90% is achieved for inferring the range of values for $\theta_{l,2}$ across the majority area of the entire region. A few areas with inaccurate inference may be attributed to the complexity of the scattering environment.

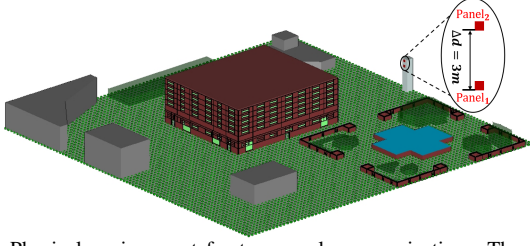


Fig. 5. Physical environment for two-panel communications. The red little boxes are Panel₁ and Panel₂. The green little squares that cover the entire area are UE locations, and they are spaced 2.5 meters apart. The large red and gray objects are buildings. The green irregular objects are vegetation, and the blue area is the pond.

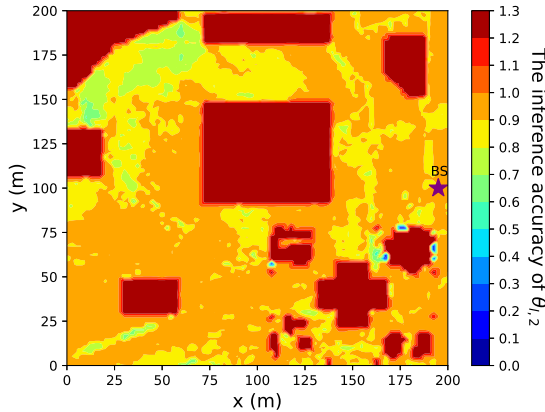


Fig. 6. The accuracy for inferring $\theta_{l,2}$ for multi-path sharing near-field scatterers scenario with $\delta = 0.15$ meters.

V. CONCLUSION

In this letter, we study the problem of channel inference where the BS is equipped with two antenna panels that may use different frequency bands for communication. Four different scenarios are considered, namely far-field free-space, near-field free-space, multi-path sharing far-field scatterers, and multi-path sharing near-field scatterers. Simulation results based on ray-tracing in a realistic radio propagation environment demonstrate that the channel of one panel can be in principle fully inferred from that of the other panel for both far-field and near-field free-space scenarios. On the other hand, for the multi-path scenarios sharing far-field or near-field scatterers, the angles or range of angles of the MPCs can be inferred, respectively.

APPENDIX A

PROOF OF THE INFERENCE OF $\alpha(\lambda_2)$ IN (7)

Based on the expression (6), $\alpha(\lambda_2) = \frac{\lambda_2}{4\pi R_2} e^{-\frac{j2\pi R_2}{\lambda_2}}$, where

$$\frac{\lambda_2}{4\pi R_2} = \frac{\lambda_1}{4\pi R_1} \frac{\lambda_2 R_1}{\lambda_1 R_2} \approx \frac{\lambda_1}{4\pi R_1} \frac{\lambda_2}{\lambda_1} = |\alpha(\lambda_1)| \frac{\lambda_2}{\lambda_1}, \quad (13)$$

$$\begin{aligned} e^{-\frac{j2\pi R_2}{\lambda_2}} &= e^{-\frac{j2\pi(R_1 - \Delta d \sin(\theta_2))}{\lambda_2}} = \left(e^{-\frac{j2\pi R_1}{\lambda_1}} \right)^{\frac{\lambda_1}{\lambda_2}} e^{\frac{j2\pi \Delta d \sin(\theta_2)}{\lambda_2}} \\ &= \left(\frac{\alpha(\lambda_1)}{|\alpha(\lambda_1)|} \right)^{\frac{\lambda_1}{\lambda_2}} e^{\frac{j2\pi \Delta d \sin(\theta_2)}{\lambda_2}}. \end{aligned} \quad (14)$$

The approximation in equations (13) follows by letting $R_1 \approx R_2$ when evaluating the amplitude for far-field scenario, and the range of θ_2 in equations (14) is $(-\frac{\pi}{2}, 0)$. Therefore, the inference of $\alpha(\lambda_2)$ in (7) is proved.

REFERENCES

- [1] R. W. Heath, N. Gonzalez-Prelcic, S. Rangan, W. Roh, and A. M. Sayeed, "An overview of signal processing techniques for millimeter wave MIMO systems," *IEEE J. Sel. Topics Signal Process.*, vol. 10, no. 3, pp. 436–453, Apr. 2016.
- [2] 3GPP, "Antenna structure: Impact on MIMO transmission and remaining modeling issues," 3rd Generation Partnership Project (3GPP), Tech. Rep. R1-166109, Aug. 2016.
- [3] W. Wang and W. Zhang, "Orthogonal projection-based channel estimation for multi-panel millimeter wave MIMO," *IEEE Trans. Commun.*, vol. 68, no. 4, pp. 2173–2187, Apr. 2020.
- [4] 3GPP, "Multi-panel/multi-TRP transmission," 3rd Generation Partnership Project (3GPP), Tech. Rep. R1-1702071, Feb. 2017.
- [5] S. Zhang, S. Zhang, J. Ma, T. Liu, and O. A. Dobre, "Deep learning based antenna-time domain channel extrapolation for hybrid mmWave massive MIMO," *IEEE Trans. Veh. Technol.*, vol. 71, no. 12, pp. 13398–13402, Dec. 2022.
- [6] M. Alrabeiah and A. Alkhateeb, "Deep learning for TDD and FDD massive MIMO: Mapping channels in space and frequency," in *Proc. 53rd Asilomar Conf. Signals Syst. Comput.*, May 2019, pp. 1465–1470.
- [7] A. Ali, N. Gonzalez-Prelcic, and R. W. Heath, "Spatial covariance estimation for millimeter wave hybrid systems using out-of-band information," *IEEE Trans. Wireless Commun.*, vol. 18, no. 12, pp. 5471–5485, Dec. 2019.
- [8] B. Lin, F. Gao, S. Zhang, T. Zhou, and A. Alkhateeb, "Deep learning-based antenna selection and CSI extrapolation in massive MIMO systems," *IEEE Trans. Wireless Commun.*, vol. 20, no. 11, pp. 7669–7681, Nov. 2021.
- [9] S. Chen, Z. Jiang, J. Liu, R. Vannithamby, S. Zhou, Z. Niu, and Y. Wu, "Remote channel inference for beamforming in ultra-dense hypercellular network," in *Proc. IEEE Global Commun. Conf. (GLOBECOM)*, Dec. 2017, pp. 1–6.
- [10] W. Wang, W. Zhang, Y. Li, and J. Lu, "Channel estimation and hybrid precoding for multi-panel millimeter wave MIMO," in *Proc. IEEE Int. Conf. Commun. (ICC)*, 2018, pp. 1–6.
- [11] Z. Zhang, J. Zhang, Y. Zhang, L. Yu, and G. Liu, "AI-based time-, frequency-, and space-domain channel extrapolation for 6G: Opportunities and challenges," *IEEE Veh. Technol. Mag.*, Mar. 2023.
- [12] Y. Zeng and X. Xu, "Toward environment-aware 6G communications via channel knowledge map," *IEEE Wireless Commun.*, vol. 28, no. 3, pp. 84–91, 2021.
- [13] Y. Zeng, J. Chen, J. Xu, D. Wu, X. Xu, S. Jin, X. Gao, D. Gesbert, S. Cui, and R. Zhang, "A Tutorial on Environment-Aware Communications via Channel Knowledge Map for 6G," accepted by *IEEE Commun. Survey & Tutorials*, available on arXiv. <https://arxiv.org/abs/2309.07460>.
- [14] R. Schmidt, "Multiple emitter location and signal parameter estimation," *IEEE Trans. Antennas Propag.*, vol. 34, no. 3, pp. 276–280, Mar. 1986.
- [15] J. A. Fessler and A. O. Hero, "Space-alternating generalized expectation-maximization algorithm," *IEEE Trans. Signal Process.*, vol. 42, no. 10, pp. 2664–2677, Oct. 1994.
- [16] C. Zhang, Z. Zhou, H. Wang, and Y. Zeng, "Integrated super-resolution sensing and communication with 5G NR waveform: Signal processing with uneven CPs and experiments," in *2023 21th Int. Symp. Modeling Optimization Mobile, Ad hoc Wireless Netw. Workshops (WiOpt Wkshps)*, Aug. 2023, pp. 1–8.
- [17] K. T. Selvan and R. Janaswamy, "Fraunhofer and fresnel distances: Unified derivation for aperture antennas," *IEEE Antennas Propag. Mag.*, vol. 59, no. 4, pp. 12–15, Aug. 2017.
- [18] H. Lu and Y. Zeng, "Communicating with Extremely Large-Scale Array/Surface: Unified Modelling and Performance Analysis," *IEEE Trans. Wireless Commun.*, vol. 21, no. 6, pp. 4039–4053, Jun. 2022.
- [19] D. Wu, Y. Zeng, S. Jin, and R. Zhang, "Environment-aware hybrid beamforming by leveraging channel knowledge map," *IEEE Trans. Wireless Commun.*, early access, 2023.